

1      **Dynamic driving eliminates volume fraction inhomogeneity and apparent yield stress**  
2      **in flowing dense non-Brownian suspensions**

3                    Christopher Ness<sup>1</sup> and Amgad S. Moussa<sup>2</sup>

4                    <sup>1</sup>*School of Engineering, University of Edinburgh, Edinburgh, EH9 3JL, United Kingdom*

5                    <sup>2</sup>*Syngenta Crop Protection AG, 4058 Basel, Switzerland*

6      Dense suspensions of non-Brownian hard spheres are often characterised as yield-stress fluids  
7      despite having no intrinsic time or force scales that could lead to such rheology. One mechanism  
8      for the apparent yield stress is particle migration, which produces (or is caused by) inhomogeneous  
9      flow conditions and leads to local regions where the solids content approaches or exceeds the limit  
10     of flowability. In such a scenario one does not induce flow by exceeding a yield stress, but instead  
11     by exploring the only remaining control parameter, namely the flow history. We demonstrate using  
12     particle-based simulation that this apparent local yield stress behaviour does indeed emerge in a  
13     model dense suspension of non-Brownian hard spheres and that it can be eliminated by imposing a  
14     time-varying flow field.

15      **I. INTRODUCTION**

16      Dense suspensions of micron-sized particles are com-  
17      monplace in industry, where effective modelling for de-  
18      sign and operation of processes requires accurate and re-  
19      liable material characterisation [1, 2]. In a model system  
20      of non-Brownian, non-inertial hard particles (relevant to  
21      systems with particle radius  $a \approx 1 - 10 \mu\text{m}$ ) under steady  
22      homogeneous flow, the components of the stress tensor  
23      are linear in the shear rate and are functions of the par-  
24      ticle volume fraction  $\phi$  only [3, 4]. For the shear viscosity  
25      one can therefore write  $\Sigma_{xy}/\eta\dot{\gamma} = \mathcal{F}(\phi)$ , with  $\eta$  the vis-  
26      cosity of the suspending liquid,  $\Sigma_{xy}$  the shear stress, and  
27       $\dot{\gamma}$  the shear rate. The function  $\mathcal{F}$  is typically written  
28      in a general form as  $\kappa(\phi_m - \phi)^{-\lambda}$  [5, 6] ( $\lambda \approx 2$ ) with  
29      the maximum packing fraction  $\phi_m$  the key parameter  
30      needed to describe the rheology. Importantly this fric-  
31      tional jamming point can be exceeded in some circum-  
32      stances since it is lower than the random close packing  
33      limit  $\phi_{\text{rcp}} \approx 0.64$ .  
34

35      Practitioners typically seek to characterise suspension  
36      rheology under well-controlled conditions, and use the  
37      extracted parameters to make predictions for more com-  
38      plex engineering flow scenarios. In practice this involves  
39      measuring *e.g.*  $\Sigma_{xy}$  vs  $\dot{\gamma}$  or  $\Sigma_{xy}/\dot{\gamma}$  vs  $\Sigma_{xy}$  under con-  
40      ditions in which  $\phi$  is presumed to be spatially invariant.  
41      Experiments with granular particles indeed found  
42      no yield stress below the frictional jamming point for  
43      the density-matched case in which the particle distribu-  
44      tion remains spatially uniform [3, 7]. In cases where the  
45      stress field predisposes the system to particle migration,  
46      however, this approach can prove problematic. For a non-  
47      Brownian suspension in a Couette flow, for instance, one  
48      often finds an inner sheared region and an outer annulus  
49      that is non-flowing [8, 9] (or much slower flowing [10, 11]),  
50      and similarly a yield stress is reported in granular suspen-  
51      sions for which gravity causes settling [7]. This observa-  
52      tion means that one could characterise the bulk constitu-  
53      tive behaviour of the material using a model with a finite  
54      yield stress (see the discussion in [9]), despite a simple di-  
55      mensional analysis (mentioned above, see Boyer *et al.* [3])  
56

57      demonstrating that this is not possible below  $\phi_m$ . The  
58      non-flowing region appears due to the spatially varying  
59       $\phi$  that emerges as a result of normal stress gradients, so  
60      that the e.g. Herschel-Bulkley parameters obtained from  
61      such a measurement do not describe a flow curve *per se*  
62      but rather a series of points from a family of flow curves  
63      each with different  $\phi$ . What is being measured is thus  
64      not a *local* flow rule [12, 13] or constitutive behaviour for  
65      a constant- $\phi$  material, and consequently the parameters  
66      measured under one set of flow conditions will inevitably  
67      fail to predict the flow behaviour in others. More fun-  
68      damentally, the non-flowing region is not indicative of a  
69      yield stress in a homogeneous material but rather of a  
70      spatial region in which the local  $\phi$  approaches or even  
71      exceeds the jamming value  $\phi_m$ .

72      This subtle but important distinction has consequences  
73      for how one might achieve *unjamming* in practical sce-  
74      narios, which we address here. In general, one achieves  
75      flow in a yield stress fluid by overcoming that stress. In  
76      non-Brownian suspensions in which particle migration is  
77      present, increasing the applied stress will fail to unjam  
78      the system (unless the particles are deformable). This  
79      must instead be achieved by changing the details of the  
80      flow protocol, a requirement deriving from the fragility  
81      of such materials and the tendency for their viscosity  
82      to decrease upon changes to flow direction [14–16]. Under-  
83      standing this distinction in governing physics is cru-  
84      cial to achieving flow in jammed scenarios, and has been  
85      explored in various contexts including vibration-induced  
86      liquefaction [17, 18] and in more controlled superposed  
87      orthogonal shear [19].

88      Here we explore this problem using a computational  
89      thought experiment: a particle-based simulation mod-  
90      elling the Newtonian dynamics of suspended hard spheres  
91      under various imposed inhomogeneous flow conditions,  
92      accounting for pairwise hydrodynamic lubrication and  
93      frictional particle-particle contact forces [20]. Our im-  
94      posed flow is a time-varying extension of that described  
95      by Saitoh and Tighe [21] (see also Refs [22, 23], though  
96      we address transient flows which these works do not),  
97      and sets up volume fraction profiles that locally exceed  
98

$\phi_m$ , allowing us to demonstrate and then scrutinise the apparent yield stress behaviour, before exploring under what conditions it can be eliminated.

## II. NUMERICAL MODEL

We model a non-Brownian suspension of micron-sized spheres under an imposed driving force that leads to a spatially and temporally varying shear rate  $\dot{\gamma}(y, t)$ . The particle properties that set the length, mass and time scales are the radius  $a$  [length], density  $\rho$  [mass/length<sup>3</sup>] (equal to the fluid density), and stiffness  $k_n$  [mass/time<sup>2</sup>] (this has a tangential counterpart  $k_t = 0.7k_n$ ). Also relevant are the fluid viscosity  $\eta$  [mass/(length×time)], the solid volume fraction  $\phi$  [dimensionless]; and the inter-particle friction coefficient  $\mu = 0.5$  [dimensionless]. The timescales  $\sqrt{\rho a^3/k_n}$  and  $\rho a^2/\eta$  are set  $\ll 1/\dot{\gamma}$  so that the system meets the criteria for being rate-independent, and we set  $(\rho a^2 h_{\min}/\eta)/\sqrt{\rho a^3/k_n} = 0.1$  so that contacts are fully overdamped ( $h_{\min}$  is defined below). At steady state and with spatially uniform  $\dot{\gamma}$ , the dimensionless shear stress  $\Sigma_{xy}/\eta\dot{\gamma}$  is thus a function of  $\phi$  only [3].

Particles are subject to Stokes drag, pairwise lubrication and pairwise contact forces and torques [24]. The drag on particle  $i$  (radius  $a_i$ ) is set by its velocity  $\mathbf{u}_i$  and the specified fluid streaming velocity at its centre  $\mathbf{u}^\infty(\mathbf{x}_i)$ :  $\mathbf{F}_i^d = -6\pi\eta a_i(\mathbf{u}_i - \mathbf{u}^\infty(\mathbf{x}_i))$ . Similarly, a torque acts to cause the particles to rotate with angular velocity set by  $\frac{1}{2}(\nabla \times \mathbf{u}^\infty)$ . Neighbouring particles  $i$  and  $j$  with centre-to-centre vector  $\mathbf{r}_{i,j}$  experience lubrication forces [25, 26] dependent on the dimensionless gap  $h$  between their surfaces and their relative velocity. The leading term scales with  $1/h$  and the normal component (along  $\mathbf{r}_{i,j}$ ) of the pairwise velocity difference:  $\mathbf{F}_{i,j}^l = \frac{3}{2}\pi a_i \eta \frac{1}{h}(\mathbf{u}_j - \mathbf{u}_i)_n$ . Lubrication forces oppose relative motion between particles and are prevented from diverging at contact by an imposed lower limit on  $h_{\min} = 10^{-3}$  (with results insensitive to this choice when  $10^{-4} < h_{\min} < 10^{-2}$ ). A torque also acts to resist relative rotation between  $i$  and  $j$ , detailed elsewhere [20]. Contacting particles  $i$  and  $j$  experience repulsive forces dependent on the scalar overlap  $\delta = 2a - |\mathbf{r}_i - \mathbf{r}_j|$  and the absolute tangential displacement accumulated over the duration of the contact  $\xi$ :  $\mathbf{F}_{i,j}^c = k_n \delta \mathbf{r}_{i,j}/|\mathbf{r}_{i,j}| - k_t \xi$ . The friction coefficient  $\mu$  sets an upper bound on  $\xi$  through  $|\xi| \leq \mu k_n \delta / k_t$ . The  $\alpha, \beta$  component of the stress  $\Sigma$  due to lubrication and contact is found, respectively, by summing  $(F_{i,j}^{l,\alpha} r_{i,j}^\beta + F_{i,j}^{l,\beta} r_{i,j}^\alpha)/2$  and  $F_{i,j}^{c,\alpha} r_{i,j}^\beta$  over all pairs. The forces are summed on each particle and the trajectories are then updated with timestep chosen to be small compared to  $\sqrt{\rho a^3/k_n}$  and  $\rho a^2/\eta$ .

$L_y = 100a, 200a, 400a$  (Fig. 1(a)) so that there is scale separation between the domain size in the velocity gradient direction and the particle, and we initialise the system with a spatially homogeneous volume fraction of  $\bar{\phi} = 0.59$  (fractionally below the simple shear jamming point, see below). Simulations comprise  $\approx 40000$  particles with radii  $a$  and  $1.4a$  mixed in equal numbers, chosen to prevent crystallisation while retaining rheology and jamming points close to the idealised monodisperse limit [27].

We drive flow by manipulating the per-particle Stokes drag term described above, applying a streaming velocity  $\mathbf{u}^\infty$  as

$$\mathbf{F}_i^d = -6\pi\eta a_i \left( \mathbf{u}_i - \underbrace{\alpha_1 \sin\left(\frac{2\pi y_i}{L}\right) \boldsymbol{\delta}_x}_{\mathbf{u}^\infty} \right). \quad (1)$$

Here  $y_i$  is the  $y$ -coordinate of particle  $i$  and  $\boldsymbol{\delta}_x$  is a unit vector pointing along  $x$ . This  $\mathbf{u}^\infty$  is sketched in Fig. 1(a). This force introduces a timescale  $L/2\pi\alpha_1$ , which compares against the viscous timescale to give a dimensionless control parameter  $\rho(2\pi\alpha_1/L)a^2/\eta$ . Setting this quantity  $\mathcal{O}(10^{-2})$  results in local Stokes numbers  $\rho\dot{\gamma}(y)a^2/\eta \leq 10^{-2}$  so that particle inertia can be neglected. In this range shear rates and stresses scale linearly with  $\alpha_1$  (equivalent to the rate-independent result for simple shear [3]). We focus first on the steady-state behaviour, before addressing the dynamics associated with start-up and time-varying driving.

Shown in Fig. 1(b)-(e) are steady state profiles in  $y$  of the normal  $\Sigma_{yy}$  and shear  $\Sigma_{xy}$  stresses rescaled by a characteristic stress  $\eta(2\pi\alpha_1/L)$ , the shear rate  $\rho\dot{\gamma}a^2/\eta$  and the volume fraction  $\phi$ . We first demonstrate that the rheology is in violation of a local flow rule, having obtained the latter using simple shear simulations with  $\mathbf{F}_i^d = -6\pi\eta a_i(\mathbf{u}_i - \dot{\Gamma}y_i/L\boldsymbol{\delta}_x)$  for constant  $\dot{\Gamma}$  and varying  $\phi$ . In Fig. 1(f) are homogeneous shear and normal stresses, with solid lines showing fits to  $\Sigma_{yy}/\eta\dot{\gamma} = \tilde{\kappa}(\phi_m - \phi)^{-2}$  and  $\Sigma_{xy}/\eta\dot{\gamma} = \kappa(\phi_m - \phi)^{-2}$ , with  $\phi_m = 0.595$ ,  $\tilde{\kappa} = 0.15$  and  $\kappa = 0.09$ . Using the measured, spatially-uniform normal stresses from inhomogeneous flow (from Fig. 1(b)) and the imposed  $\mathbf{u}^\infty$  (grey line Fig. 1(d)) we predict the profiles in  $y$  of volume fraction  $\phi(y) = \phi_m - (\tilde{\kappa}\eta|\dot{\gamma}(y)|/\Sigma_{yy})^{1/2}$  and shear stress  $\Sigma_{xy}(y) = \kappa\eta\dot{\gamma}(\phi_m - \phi(y))^{-2}$  (broad lines in Figs. 1(c),(e)). Despite being bound by  $\phi_m$  as the maximum allowed value of  $\phi$  and having to conform to the imposed shear rate, the local assumption makes reasonable predictions of  $\phi(y)$  and  $\Sigma_{xy}(y)$  in regions where  $\rho\dot{\gamma}(y)a^2/\eta$  is large, but around  $y/L = 0.25, 0.75$  it fails dramatically. In particular, the measured  $\phi$  is able to exceed significantly the homogeneous  $\phi_m$  in large regions of the domain (though it remains bounded by the close-packing limit  $\phi_{rcp} \approx 0.64$ ), confirming that the local flow rule measured under homogeneous conditions does not apply (measuring  $\phi_m$  with greater precision would not change this conclusion). These regions have very low shear rate and are indicative of narrow plug-like regions. The spatial variation

## III. STEADY STATE INHOMOGENEOUS FLOW

For inhomogeneous flow simulations we set the periodic simulation box size as  $L_x = 60a$ ,  $L_z = 20a$ , with

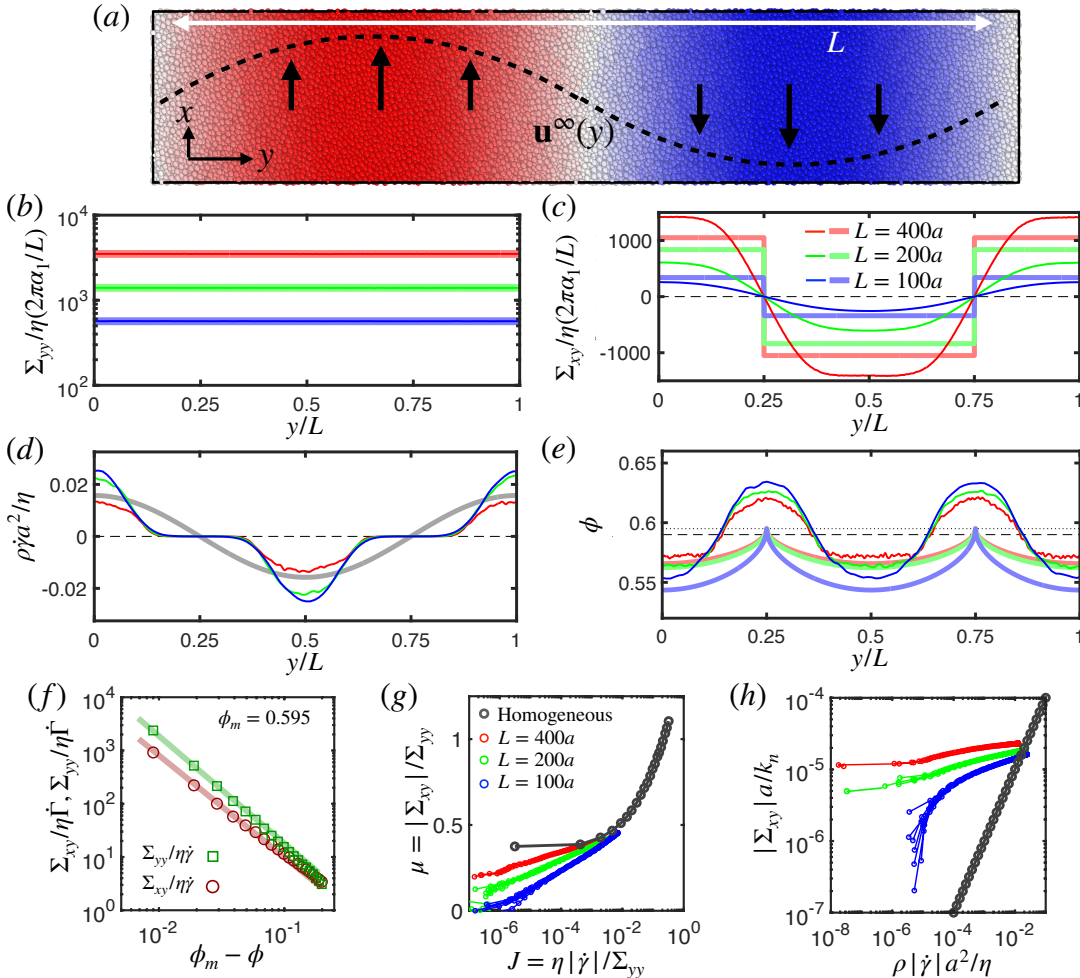


FIG. 1. Steady state inhomogeneous flow. (a) Snapshot of simulation. Dashed line indicates the magnitude of the streaming velocity applied to each particle according to its  $y$  position, with small arrows and colour scale indicating the flow direction. Shown in (b)-(e) are profiles in  $y$  of, respectively, the normal stress  $\Sigma_{yy}/\eta(2\pi\alpha_1/L)$ ; the shear stress  $\Sigma_{xy}/\eta(2\pi\alpha_1/L)$ ; the dimensionless shear rate  $\rho\dot{\gamma}a^2/\eta$ ; and the volume fraction  $\phi$  (with the black dashed line in (e) indicating the mean  $\bar{\phi} = 0.59$  and the dotted line indicating  $\phi_m = 0.595$ , with  $L = 400a$  (red),  $L = 200a$  (green),  $L = 100a$  (blue)). Broad coloured lines in (b), (c), (e) represent predictions of the local constitutive model described in the text, assuming the flow follows the imposed  $\mathbf{u}^\infty$  (grey line in (d)). (f) Local rheology measured with  $\rho\dot{\gamma}a^2/\eta = 0.01$ , showing the shear (red) and normal (green) stresses as functions of  $\phi$ . Solid lines are fits to the local model described in the text. In (g) and (h) are rheology data presented parametrically as  $\mu(y)$  vs.  $J(y)$  and  $|\Sigma_{xy}(y)|a/k_n$  vs.  $\rho|\dot{\gamma}(y)|a^2\eta$ . Grey points and lines indicate homogeneous data; coloured lines represent inhomogeneous data with different  $L$  (colours as above) with each point representing a  $y$  position.

of  $\phi$  emerges as a consequence of a transient gradient in the normal stress  $\Sigma_{yy}$  during start up [10]. In the steady state, once the  $\phi$  profile has established,  $\Sigma_{yy}$  is uniform across  $y$  (Fig. 1(b)).

Representative flow curves obtained under steady state sinusoidal driving are shown parametrically in Figs. 1(g)-(h). In Fig. 1(g) is the ' $\mu(J)$ '-rheology under inhomogeneous flow (colors) compared against simple shear (grey), where the latter corresponds well to canonical experiments [3]. Here each colored point represents a binned region in  $y$  of width  $\approx a$ , with each plotted point thus representing a different volume fraction. Consistent with the  $y$ -profiles (Figs. 1(b)-(e)), inhomogeneous data violate the simple shear rheology when the shear rate is low,

with  $L = 100a$  data reaching  $\mu = 0$  and data for larger system sizes consistently decreasing with shear rate over the range of accessible  $J$ . Figure 1(h) plots the local reduced shear stress  $|\Sigma_{xy}|a/k_n$  versus the local shear rate  $\rho\dot{\gamma}(y)a^2/\eta$ , again with each plotted point representing a specific  $y$ -coordinate and thus having a different volume fraction. Each plotted point thus represents a single point taken from one of a family of volume fraction-dependent homogeneous constitutive curves, with an example given in grey for the global volume fraction of the system. For  $L = 400a$  the inhomogeneous data clearly tend towards an apparent yield stress as  $\dot{\gamma} \rightarrow 0$  (noting that  $\Sigma_{xy} = 0$  precisely at the spatial position where  $\dot{\gamma} = 0$ ), whereas this effect is weakened as the gradient

of the driving flow is increased, suggesting that the importance of the apparent yield stress and its behaviour under dynamic flow described below becomes more important in larger geometries. (Indeed most practical geometries in which dense suspensions arise will have shear rate gradients spanning lengthscales much larger than  $\mathcal{O}(100a)$ .) Importantly, the data in Fig. 1(h) is not a true flow curve: each data point is measured at a different  $y$  position, for which the local  $\phi$  is varying according to Fig. 1(e). Rather, we are plotting a series of points each taken from a separate rate-independent flow curve. Nonetheless, what is important is that in this representation the viscosity diverges as the shear rate is lowered (equivalently  $\Sigma_{xy} \rightarrow \text{constant}$  as  $\dot{\gamma} \rightarrow 0$ ) and  $\phi > \phi_m$ , superficially representing yield stress behaviour. This phenomenology is occurring for  $\bar{\phi} = 0.59$ , where under homogeneous conditions the material flows viscously (albeit with large viscosity).

#### IV. TRANSIENT FLOW

Following the reasoning that leads to rate-independence in steady states for non-Brownian suspensions, one finds that the stress may also depend on the flow history. This is well-supported by experimental data, notably the pioneering flow-reversal experiments of Gadala-Maria and Acrivos [28], and later demonstrations that time-varying flow can reduce the viscosity of shear thickening suspensions [19]. From this we infer that time-varying flow fields can produce behaviour that violates the steady state (homogeneous or inhomogeneous) rheology, a result that is well-established in spatially uniform flows [19, 29]. A central question to the latter works is how fast does the flow need to vary in order to produce novelty.

In the absence of other time or force scales (thermal motion, attractive or repulsive interactions), the only relevant timescale in our model is the time taken to establish the inhomogeneous volume fraction profile  $\phi(y)$  shown in Fig. 1(e). Since we are operating under rate-independent conditions (i.e. since  $\rho\dot{\gamma}a^2/\eta$  is small) it is more appropriate to consider the strain taken to establish the  $\phi$  profile, since (in the linear regime) the time taken will scale inversely with the characteristic timescale for driving flow in our model,  $L/2\pi\alpha_1$ .

To determine the rate at which our system advances towards spatially inhomogeneous steady states, we consider start-up flow during the transient period from  $t = 0$  (when the particle distribution is uniform in space) up until the steady states in Fig. 1 are reached, Fig. 2. Starting from a homogeneous particle distribution ( $\phi \neq \phi(y)$ ) with no shear ( $\dot{\gamma}(y) = 0$ ), the system reaches an established  $\phi(y)$  profile once the elapsed time is such that  $(2\pi\alpha_1/L)t \approx 1$ , corresponding to a strain of  $\approx 1$  along the sheared regions. Over the same duration one observes the normal stress obtaining a spatially uniform value, indicating that beyond  $\dot{\gamma}t = 1$  there is no driving force for

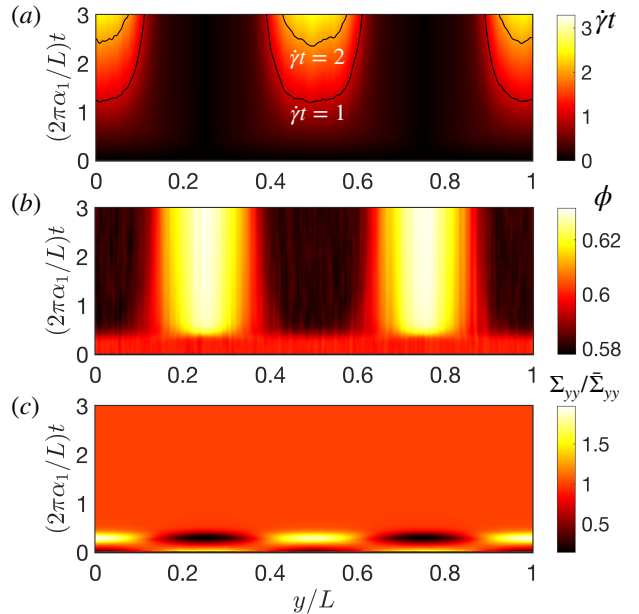


FIG. 2. Time series of the initial transient after starting up from a spatially-uniform state. Horizontal axis represents the spatial position in  $y$ ; vertical axis is increasing time  $t$ ; color bar gives the accumulated strain (a) and volume fraction (b) and normal stress (c) profiles. (a) Accumulated strain profile  $|\dot{\gamma}(y)|t$ , showing a steady increase in the strain along  $y/L = 0, 0.5, 1$  and no accumulated strain in the regions at  $y/L = 0.25, 0.75$  where  $\dot{\gamma} \approx 0$ . Solid black lines are contours at integer values of  $\dot{\gamma}t$ . (b) Development of volume fraction profile  $\phi(y)$  with time. The time  $t$  on the vertical axis is scaled with the characteristic time associated with driving,  $L/2\pi\alpha_1$ . (c) Development of the uniform normal stress profile  $\Sigma_{yy}(y)$  occurs within the initial 0.5 strain units, consistent with the evolution of the  $\phi$  field. Here  $\Sigma_{yy}$  is rescaled by its spatially averaged value at each timestep  $\bar{\Sigma}_{yy}$ .

further particle migration.

In order to disrupt particle migration and mitigate against regions with  $\phi > \phi_m$ , one must introduce a driving flow that changes its position more rapidly than the inhomogeneous volume fraction profile can establish. Defining a characteristic velocity scale for the time-varying driving as  $\alpha_2$  (see below), we might expect such dynamic driving to influence the steady state particle distribution when  $\alpha_2/\alpha_1 \gtrsim 1$ . This dimensionless ratio operates in some sense as a Peclet number, comparing the size of the fluctuations or perturbations to the system to the translation driven by the mean flow. Works that applied vibrations to granular packings in other settings similarly found that increasing the magnitude of imposed noise (analogous but not identical to our moving flow field) resulted in liquefaction of the material [17, 30].

#### V. DYNAMIC INHOMOGENEOUS FLOW

To test this idea we apply a time-varying driving force,

given by a modified version of the drag used above:

$$\mathbf{F}_i^d = -6\pi\eta a_i \left( \mathbf{u}_i - \alpha_1 \sin\left(\frac{2\pi}{L}(y_i + \alpha_2 t)\right) \boldsymbol{\delta}_x \right). \quad (2)$$

This form (sketched in Fig. 3(a)) is chosen as the most simple way to introduce time-dependence into the model beyond the initial transient. It produces a sinusoidal form for  $\mathbf{u}^\infty$  that translates in the  $+y$  direction with constant velocity set by  $\alpha_2$ . The nature of the flow is then given by a competition between the downstream flow driving determined by  $\alpha_1$ , and the rate of change of the flow direction determined by  $\alpha_2$ . Importantly, it is not sufficient to simply vary  $\alpha_1$  in time with  $\alpha_2 = 0$ . The resulting ‘pulsed’ flow would, under rate-independent conditions, not lead to a change in the net path followed by particles (it would only change the rate at which their path is followed) so would not change the bulk rheology in Figs. 1(g)-(h).

Shown in Fig. 3(b)-(e) are steady state results for  $\alpha_2/\alpha_1 = [0, 1]$ , where the horizontal axes in (b) and (c) are shifted so that  $y/L = 0$  maps to  $\mathbf{F}_i^d = 0$ . In each case we initialised the system with  $\alpha_2 = 0$  so that  $\phi$  locally exceeded  $\phi_m$ . Focussing on the volume fraction profile  $\phi(y)$ , Fig. 3(b), we see that increasing  $\alpha_2/\alpha_1$  leads to a homogenisation of the system, *i.e.*  $\phi(y)$  becoming spatially uniform. This is associated with the shear rate profile more closely following the imposed affine flow, Fig. 3(c). For  $\alpha_2/\alpha_1 = 0.1$ ,  $\phi(y)$  becomes distorted with the peaks being lowered and shifted. The phase shift in the  $\phi$  peaks is explainable in terms of a momentum balance per unit volume in  $y$  taken from a reference point moving at  $\alpha_2$ . For  $\alpha_2 = 0$  one obtains steady states when the  $\dot{\gamma}$  and  $\phi$  profiles are such that  $\frac{\partial}{\partial y} \Sigma_{yy} = 0$  (though the non-local constitutive relation governing this balance is elusive). Here the symmetry is such that positions in space separated by  $y/L = 0.25$  are equivalent up to a factor  $\pm 1$ . For  $\alpha_2 \neq 0$ ,  $\frac{\partial}{\partial y} \Sigma_{yy}$  at each  $y$  position must balance the change in momentum associated with a flux through that position with rate  $\alpha_2$  but time-varying  $\phi$ . This leads to  $\phi$  and  $\dot{\gamma}$  becoming out of phase, Fig. 3(d), so that the symmetry is broken and instead positions separated by  $y/L = 0.5$  are equivalent. At  $\alpha_2/\alpha_1 = 1$  the system is completely homogeneous in terms of the particle distribution in  $y$ .

This change in the arrangement of particles is reflected in the measured rheology. Plotting the stress against strain rate, Fig. 3(e), we see a progressive shift from the apparent yield stress behaviour to a more rate-dependent response when  $\alpha_2/\alpha_1 = 1$ . In the latter case the two branches of the flow curve (in pink) show the stress increasing with shear rate (both being approximately linear over a narrow range), with the stress at all shear rates being lower than the simple shear one obtained at the same global volume fraction (shown in light grey). The rheology here is bivalued since the breaking of symmetry described above leads to states of distinct  $\phi$  (separated by  $y/L = 0.25$ ) sharing a common  $|\dot{\gamma}|$ . Here the rapidly changing driving flow acts similarly to the

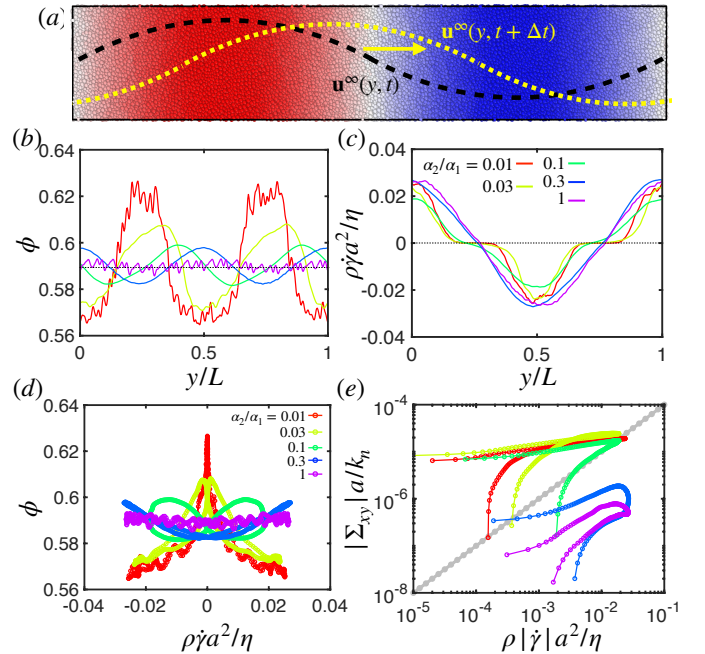


FIG. 3. Response to driving with a spatially and temporally varying  $\mathbf{u}^\infty$ . (a) Snapshot of the simulation showing the applied driving  $\mathbf{u}^\infty(y)$  at time  $t$  in black and at some later time  $t + \Delta t$  in yellow; (b) volume fraction profiles  $\phi(y)$  for varying  $\alpha_2/\alpha_1$  (see legend in (c)); (c) shear rate profiles  $\rho\dot{\gamma}a^2/\eta$  for varying  $\alpha_2/\alpha_1$ ; (d) Phase shift in  $\phi, \dot{\gamma}$  for varying  $\alpha_2/\alpha_1$ ; (e) apparent flow curves obtained by parametric plots of  $|\Sigma_{xy}(y)|a/k_n$  vs.  $\rho|\dot{\gamma}(y)|a^2\eta$  for varying  $\alpha_2/\alpha_1$ , with grey line indicating homogeneous result.

vibrations described by [17] and the orthogonal shear described by [19], that is, perturbing the instantaneous shear rate sufficiently fast that a steady microstructure cannot establish. Thus by changing the flow field rapidly we demonstrate and utilise the flow-history dependence of the material, noting that the relevant competition of timescales does not involve an internal material relaxation time (as would be the case in a thixotropic material) but rather the ratio of the driving timescales represented by  $\alpha$ . In the inhomogeneous flow presented here the comparatively rapid perturbation at large  $\alpha$  has the additional effect of homogenising the volume fraction profile. Recognising that the response time to changes of flow direction decreases with increasing proximity to jamming [31], it is likely that the value of  $\alpha$  needed to eliminate the apparent yield stress will increase with the global volume fraction of the system, though this dependence is likely to be complex and warrants further investigation. Similarly, other factors that influence the position of the jamming point of the system such as polydispersity [27] and particle shape [32] will be important in governing the responsiveness of the material to dynamic inhomogeneous driving.

380

## VI. CONCLUDING REMARKS

396

397

We have shown that inhomogeneous flow in dense non-Brownian suspensions drives particle migration, leading to a spatially varying volume fraction that can locally exceed the simple shear frictional jamming point  $\phi_m$  by a significant amount. This effect can be eliminated by imposing a time-varying flow, choosing the timescale for the variation to be shorter than the characteristic time required for the spatial  $\phi$  profile to establish. Importantly, achieving elimination of the apparent yield stress does not require us to exceed any critical stress (indeed, we can make our flow rates arbitrarily small by manipulating the parameter  $\alpha_1$ , providing its ratio to  $\alpha_2$  is set appropriately). This illustrates important issues related to the flow physics of non-Brownian hard sphere suspensions: while the steady state homogeneous rheology

- [1] C. Ness, R. Seto, and R. Mari, Annual Review of Condensed Matter Physics **13**, 97 (2022).
- [2] J. J. Stickel and R. L. Powell, Annual Review of Fluid Mechanics **37**, 129 (2005).
- [3] F. Boyer, É. Guazzelli, and O. Pouliquen, Physical Review Letters **107**, 188301 (2011).
- [4] É. Guazzelli and O. Pouliquen, Journal of Fluid Mechanics **852** (2018).
- [5] I. M. Krieger and T. J. Dougherty, Transactions of the Society of Rheology **3**, 137 (1959).
- [6] S. Mueller, E. Llewellyn, and H. Mader, Proceedings of the Royal Society A: Mathematical, Physical and Engineering Sciences **466**, 1201 (2010).
- [7] A. Fall, F. Bertrand, G. Ovarlez, and D. Bonn, Physical review letters **103**, 178301 (2009).
- [8] D. Leighton and A. Acrivos, Journal of Fluid Mechanics **181**, 415 (1987).
- [9] G. Ovarlez, F. Bertrand, and S. Rodts, Journal of Rheology **50**, 259 (2006).
- [10] J. F. Morris and F. Boulay, Journal of Rheology **43**, 1213 (1999).
- [11] R. J. Phillips, R. C. Armstrong, R. A. Brown, A. L. Graham, and J. R. Abbott, Physics of Fluids A: Fluid Dynamics **4**, 30 (1992).
- [12] K. Kamrin and G. Koval, Physical Review Letters **108**, 178301 (2012).
- [13] M. Bouzid, M. Trulsson, P. Claudin, E. Clément, and B. Andreotti, Physical Review Letters **111**, 238301 (2013).
- [14] M. Cates, J. Wittmer, J.-P. Bouchaud, and P. Claudin, Physical Review Letters **81**, 1841 (1998).
- [15] F. Peters, G. Ghigliotti, S. Gallier, F. Blanc, E. Lemaire, and L. Lobry, Journal of Rheology **60**, 715 (2016).
- [16] V. G. Kolli, E. J. Pollauf, and F. Gadala-Maria, Journal of Rheology **46**, 321 (2002).
- [17] C. Hanotin, S. K. De Richter, P. Marchal, L. J. Michot, and C. Baravian, Physical Review Letters **108**, 198301 (2012).
- [18] P. Sehgal, M. Ramaswamy, I. Cohen, and B. J. Kirby,

- [19] N. Y. C. Lin, C. Ness, M. E. Cates, J. Sun, and I. Cohen, Proceedings of the National Academy of Sciences **113**, 10774 (2016).
- [20] O. Cheal and C. Ness, Journal of Rheology **62**, 501 (2018).
- [21] K. Saitoh and B. P. Tighe, Physical Review Letters **122**, 188001 (2019).
- [22] J. J. Gillissen and C. Ness, Physical Review Letters **125**, 184503 (2020).
- [23] B. P. Bhowmik and C. Ness, Physical Review Letters **132**, 118203 (2024).
- [24] C. Ness, Computational Particle Mechanics **10**, 2031 (2023).
- [25] S. Kim and S. J. Karrila, *Microhydrodynamics: principles and selected applications* (Butterworth Heinemann, 1991).
- [26] D. Jeffrey, Physics of Fluids A: Fluid Dynamics **4**, 16 (1992).
- [27] R. S. Farr and R. D. Groot, The Journal of chemical physics **131** (2009).
- [28] F. Gadala-Maria and A. Acrivos, Journal of Rheology **24**, 799 (1980).
- [29] R. Niu, M. Ramaswamy, C. Ness, A. Shetty, and I. Cohen, Science Advances **6**, eaay6661 (2020).
- [30] C. Garat, S. Kiesgen de Richter, P. Lidon, A. Colin, and G. Ovarlez, Journal of Rheology **66**, 237 (2022).
- [31] C. Ness and J. Sun, Physical Review E **93**, 012604 (2016).
- [32] N. M. James, H. Xue, M. Goyal, and H. M. Jaeger, Soft matter **15**, 3649 (2019).
- [33] H. Yoon, D. Hill, S. Balachandar, R. Adrian, and M. Ha, Chemical Engineering Science **60**, 3169 (2005).
- [34] R. Cabiscol, T. Jansen, M. Marigo, and C. Ness, Powder Technology **384**, 542 (2021).
- [35] Y. S. Tanneru, J. H. Finke, C. Schilde, Y. M. Harshe, and A. Kwade, Powder Technology , 120060 (2024).
- [36] A. Hosoi and D. I. Goldman, Annual Review of Fluid Mechanics **47**, 431 (2015).

398

- [37] C. Ness, R. Seto, and R. Mari, Annual Review of Condensed Matter Physics **13**, 97 (2022).
- [38] J. J. Stickel and R. L. Powell, Annual Review of Fluid Mechanics **37**, 129 (2005).
- [39] F. Boyer, É. Guazzelli, and O. Pouliquen, Physical Review Letters **107**, 188301 (2011).
- [40] É. Guazzelli and O. Pouliquen, Journal of Fluid Mechanics **852** (2018).
- [41] I. M. Krieger and T. J. Dougherty, Transactions of the Society of Rheology **3**, 137 (1959).
- [42] S. Mueller, E. Llewellyn, and H. Mader, Proceedings of the Royal Society A: Mathematical, Physical and Engineering Sciences **466**, 1201 (2010).
- [43] A. Fall, F. Bertrand, G. Ovarlez, and D. Bonn, Physical review letters **103**, 178301 (2009).
- [44] D. Leighton and A. Acrivos, Journal of Fluid Mechanics **181**, 415 (1987).
- [45] G. Ovarlez, F. Bertrand, and S. Rodts, Journal of Rheology **50**, 259 (2006).
- [46] J. F. Morris and F. Boulay, Journal of Rheology **43**, 1213 (1999).
- [47] R. J. Phillips, R. C. Armstrong, R. A. Brown, A. L. Graham, and J. R. Abbott, Physics of Fluids A: Fluid Dynamics **4**, 30 (1992).
- [48] K. Kamrin and G. Koval, Physical Review Letters **108**, 178301 (2012).
- [49] M. Bouzid, M. Trulsson, P. Claudin, E. Clément, and B. Andreotti, Physical Review Letters **111**, 238301 (2013).
- [50] M. Cates, J. Wittmer, J.-P. Bouchaud, and P. Claudin, Physical Review Letters **81**, 1841 (1998).
- [51] F. Peters, G. Ghigliotti, S. Gallier, F. Blanc, E. Lemaire, and L. Lobry, Journal of Rheology **60**, 715 (2016).
- [52] V. G. Kolli, E. J. Pollauf, and F. Gadala-Maria, Journal of Rheology **46**, 321 (2002).
- [53] C. Hanotin, S. K. De Richter, P. Marchal, L. J. Michot, and C. Baravian, Physical Review Letters **108**, 198301 (2012).
- [54] P. Sehgal, M. Ramaswamy, I. Cohen, and B. J. Kirby,

- [55] We have shown that inhomogeneous flow in dense non-Brownian suspensions drives particle migration, leading to a spatially varying volume fraction that can locally exceed the simple shear frictional jamming point  $\phi_m$  by a significant amount. This effect can be eliminated by imposing a time-varying flow, choosing the timescale for the variation to be shorter than the characteristic time required for the spatial  $\phi$  profile to establish. Importantly, achieving elimination of the apparent yield stress does not require us to exceed any critical stress (indeed, we can make our flow rates arbitrarily small by manipulating the parameter  $\alpha_1$ , providing its ratio to  $\alpha_2$  is set appropriately). This illustrates important issues related to the flow physics of non-Brownian hard sphere suspensions: while the steady state homogeneous rheology
- [56] is becoming well-characterised and well-understood (including links to rate-dependent phenomena such as shear thickening), inhomogeneous flow, and in particular time-dependent inhomogeneous flows, pose a major challenge to modelling and flow prediction [22]. This has direct consequences for industrial practice where knowing the relevant scale of the parameter  $\alpha$  might guide the design of baffles or impellers in stirred tanks [33] or milling processes (for which particle-based simulation is increasingly providing mechanistic insight [34, 35]), and may have far-reaching implications for fields as diverse as understanding translocation in biological systems [36].

- [57] CN acknowledges support from the Royal Academy of Engineering under the Research Fellowship scheme. The data that support the findings of this study are available from the corresponding author upon reasonable request.